AIR FLOW ANALYSIS OF THE CAMFIL CITY-M AIR PURIFIER

DR KEVIN NOLAN

School of Mechanical and Materials Engineering,
University College Dublin

Abstract. This work concerns an evaluation of the Camfil City-M air purifier performance on two fronts. The first concerns the flow kinematics associated with the device and the second the aerosol filtration capability. The flow kinematics are investigated using a novel approach to the Particle Image Velocimetry employing ultra-high resolution video to extract flow fields over $2m$ in length. This allows the room-scale dynamics of the device to be interrogated. The aerosol filtration measurements employ particle counting and laser scattering quantification to determine the filtrating efficiency of the device. While the flow kinematics suggest that the City-M can potentially filter on a 90 second cycle the aerosol measurements show that the unit robustly removes aerosol in less than 200 seconds.

1. Introduction

There has been ongoing debate throughout the SARS-CoV-2 pandemic on the airborne transmission of the virus via respiratory droplets and aerosol. The World Health Organisation has been slow to change their guidance on the issue in spite of growing evidence [1, 2, 3]. Research has shown that the virus can persist in 2–3μm particles for up to 16 hours when maintained in a rotating drum to prevent surface deposition [4]. The mean residency time of aerosol varies as a function of droplet diameter with particle diameters of 10μm remaining in the air for 0.7 hours [5] within a controlled environment. However indoor air is not stationary and is subject to air currents due to HVAC and human thermal plumes [6]. Respiratory aerosol in turn can remain in the air for hours [7]. Ensuring effective indoor ventilation to limit pathogen transmission is therefore in the interest of public health, notwithstanding economic benefits.

HVAC systems are increasingly found in modern buildings but many indoor environments are not ventilated. Many schools now operate with classroom windows open throughout the year [8] with limited evidence to the efficacy of the practise. Key to effective indoor ventilation is an understanding of room-scale flow dynamics [9] and how airflow patterns play a role in transmission, as has been throughly documented in known outbreaks [10]. Global metrics, such as air changes per hour, do not give the full picture or an understanding of how air, and any aerosol therein, is transported around a space. It is important to understand how cross-contamination, recirculation and dead volume contribute to pathogen exposure in otherwise well ventilated spaces. This requires a greater degree of analysis than is typically performed during HVAC installation that considers the indoor microclimate and movement of users of the affected space.

Retrofitting of existing HVAC systems is often prohibitively expensive and, as evidenced by prior work, does not prevent transmission from person to person within the flow path [10]. Portable air purifiers are then an attractive device to tackle these issues. Such devices are small ($< 0.1m^3$ volume), quiet, and low cost. They can offer personalised air filtration, augment existing HVAC facilities and be deployed easily.

This report evaluates the airflow performance of the Camfil City M air purifier, figure 1, in the context of room scale flow dynamics. The City M incorporates HEPA (EN1822) and activated carbon filters, features five fan speeds with an outflow at its base. Flow field measurements will be conducted to determine the effectiveness of the unit to reduce aerosol content in a test environment and also to illustrate how the the local flow field is modified during operation showing where aerosol is transported.

2. Methods

2.1. **The Particle Image Velocimetry method.** This study will make use of the Particle Image Velocimetry (PIV) technique adapted for room scale measurement in a limited fashion. PIV is a stroboscopic imaging technique where by a fluid volume, such as flow in a wind tunnel, is seeded with tracer particles [11] that faithfully follow the flow and which are subsequently tracked using 2D cross-correlation methods to produce a grid of velocity vectors that represent the kinematics of the flow. The resulting data is useful for a wide range of purposes including validating numerical simulations, quantifying flow performance of prototypes identifying flow structures and understanding the behaviours of flows for fundamental fluid mechanics research. In the context of the present study PIV measurements can reveal regions of recirculation and stagnation within a space and show how an air purifier can affect the room scale flow dynamics. Since the particles used in this study

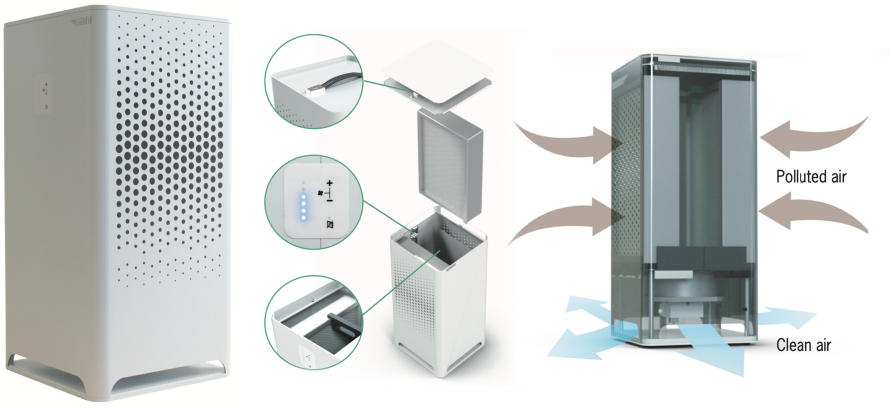

FIGURE 1. The Camfil City-M air purifier. $340 \times 720 \times 345$ mm (W×H×D)

are aerosol representative of that found due to human exhalation the will not necessarily follow the flow faithfully and will eventually fall to the ground. This may also be captured as a result.

PIV is typically deployed for small fields of view ($\ll 1m^2$) using dedicated equipment such as pulsed lasers a frame straddling cameras. Figure 2 shows a typical laboratory PIV facility comprising a dual Nd-YAG pulsed laser, data acquisition computer and frame grabber, frame straddling camera and synchronisation clock. In operation the system captures a series of images pairs of the laser illuminated slice of the flow and the particles suspended therein. The images pairs are then processed with PIV algorithms to extract the 2D flow field. The dual laser allows two laser pulses (¿100 mJ per 8 ns pulse) to be fired independent of each other and the frame straddling camera ensures that each laser pulse is acquired by separate images even at very short time differences between pulses.

Key to the PIV technique is sufficient spatial and temporal sampling. A typical PIV system has a duty cycle of 15 Hz; while time resolved systems are possible the double pulses laser and frame straddling camera ensures sufficient temporal resolution to track particles between image pairs. To achieve adequate spatial resolution requires that particles in the field of view can be tracked over a short distance so that their motion is sufficiently linear. PIV cameras typically have a $2 - 4$ MP pixel resolution, which when combined with the ability of the imaging sensor to detect scattered light from the particles limits the field of view of the technique.

To construct a flow field the image pairs are split up into a grid (often with a 50% overlap between grid squares). The grid can vary from size from 16×16 up to 128×128 pixels, usually in powers of 2 as the FFT is used for the 2D cross correlation. The 2D cross correlation compares each corresponding each pair of grid squares and the resulting correlation map used to determine the mean displacement in each grid square. The correlation map is fit with a 2D surface function to determine the sub-pixel peak location of which can increase accuracy beyond the pixel resolution of the camera. An example of this is shown in figure 3

More sophisticated variations on this method are possible and the deformation method is used herein [12]. This attempts to better capture the velocity gradient tensor of the flow by iteratively deforming one of the grid squares until the displacement vector resulting from cross correlation is

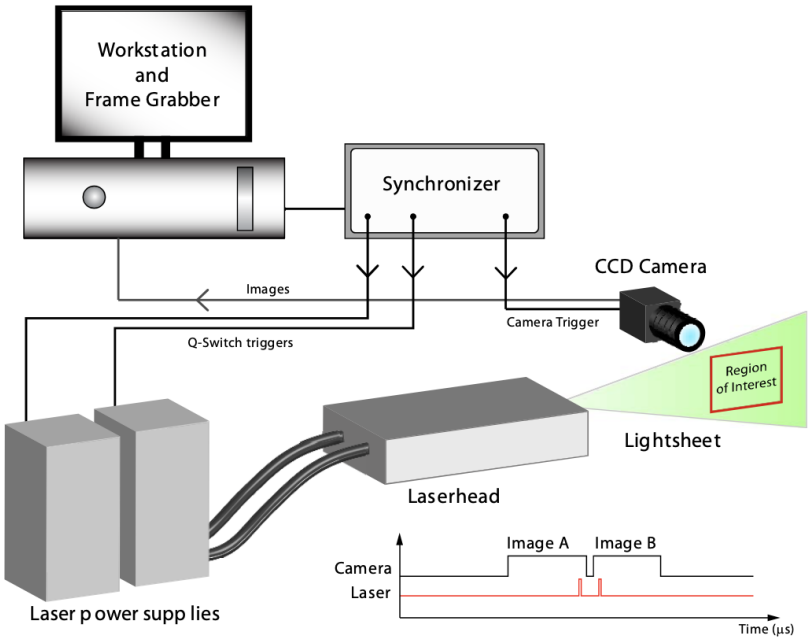

FIGURE 2. Schematic showing a typical laboratory PIV facility

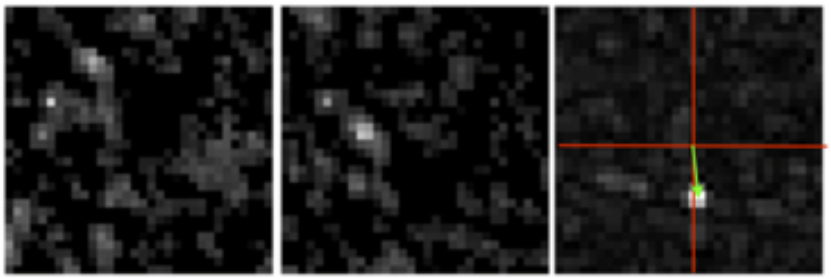

FIGURE 3. Images showing the basic principle of the PIV method, from left to right, 32×32 grid squares from an image pair and the resulting correlation map. The distance from the centre to the peak represents the mean displacement of the particles in the grid squares as show by the green vector.

zero. The final deformation is then used as the true displacement of the grid square. Applying the precise timing given by the synchroniser allows the displacement to be converted to velocity data.

The result of this processing is a 2D grid of flow vectors for each image pair. These may be further post-processed to remove spurious vectors or fill any holes. In some cases the correlation maps can be stored and secondary peaks identified as the true vector, otherwise a median filter is

employed. The resulting series of velocity vector fields may be analysed and flow statistics, such as RMS velocity, vorticity and divergence computed.

An alternative method that is suitable for steady flows is ensemble processing. Here the correlation maps are added together at each spatial location across a series of image pairs. Since the flow is steady the true peak will be reinforced relative to background noise through successive image pairs. The 2D surface fit is then applied to the final correlation map resulting in a single velocity vector field for the image sequence that may have less noise than simply averaging a series of velocity vectors.

2.2. **Large format PIV measurements.** In the current context where flow velocities are low, and in the absence of a dedicated PIV facility, flow measurements will be achieved for room scale dynamics using a low-cost approach. A continuous wave laser (2W, 532 nm) expanded into a light sheet via a 45° Powell lens is used to illuminate a 2D slice of the test environment. A ultra high-resolution camera (Canon EOS R5) capable of recording uncompressed video at 8K (8192 × 4320 pixels — 35MP) at 30 frames per second.

Aerosol was generated using a smoke wand (Concept Air Trace MK2) and an Aerogen Solo nebuliser. The former uses a propane glycol, glycerol aqueous solution while the latter employs a saline solution. The particle sizing for the smoke wand is given in figure 4 while the nebuliser produces near mono-disperse $5\mu m$ droplets.

Size Band Lower	Mid (µm)	Upper	Percentage Counts (%)		Percentage Mass (%)
0.09	0.10	0.11	19.12		3.16
0.11	0.13	0.15	39.82		14.45
0.15	0.18	0.20	23.42		20.74
0.20	0.23	0.25	10.52		19.80
0.25	0.28	0.30	4.86		16.71
0.30	0.35	0.40	1.58		11.22
0.40	0.45	0.50	0.45		6.81
0.50	0.58	0.65	0.23		7.11
0.65	0.73	0.80	0.00		0.00
0.80	0.90	1.00	0.00		0.00
1.00	1.13	1.25	0.00		0.00
1.25	1.38	1.50	0.00		0.00
1.50	1.75	2.00	0.00		0.00
2.00	2.25	2.50	0.00		0.00
2.50	2.75	3.00	0.00		0.00
Total Counts (Data):			1738	%Mass <0.5 µm	92.89
Total Counts (Background):			855	%Mass <0.7 µm	100.00
Total Counts (Data - Background):			884	%Mass <1.0 µm	100.00

FIGURE 4. Particle distribution from the Concept Air Trace MK2 smoke wand Calibration Certificate. Count Median Diameter (μm): 0.14 Mass Median Diameter (μm): 0.23 Geometric Standard Deviation: 1.50

Such an approach is effective as the flow velocities associated with ventilation flows are low and the resulting flow fields are indicative of the flow pattern and derived quantities are not required. Further measurement robustness can be obtained by ensemble averaging of the correlation data over short periods of time (100 image frames) reducing the impact of noise image non-uniform image

backgrounds at the room scale. Since this is not a frame straddling camera sequential frames will comprise the image pairs: $A \to B, B \to C, \ldots$ which is equivalent to how a time resolved system operates.

2.3. **Data gathering.** Two measurement regimes were conducted. The first was performed in a suitable space Camfil's Dublin facility, 5. Here the flow kinematics due to presence of the City-M were evaluated using the PIV method as described above using the PIVlab library for Matlab [13, 14]. The extended flow field from single and pairs of the City-M unit were evaluated. The City-M was set to its maximum speed setting for all tests herein. The video data is also available and provides insights when PIV processing was unsuccessful.

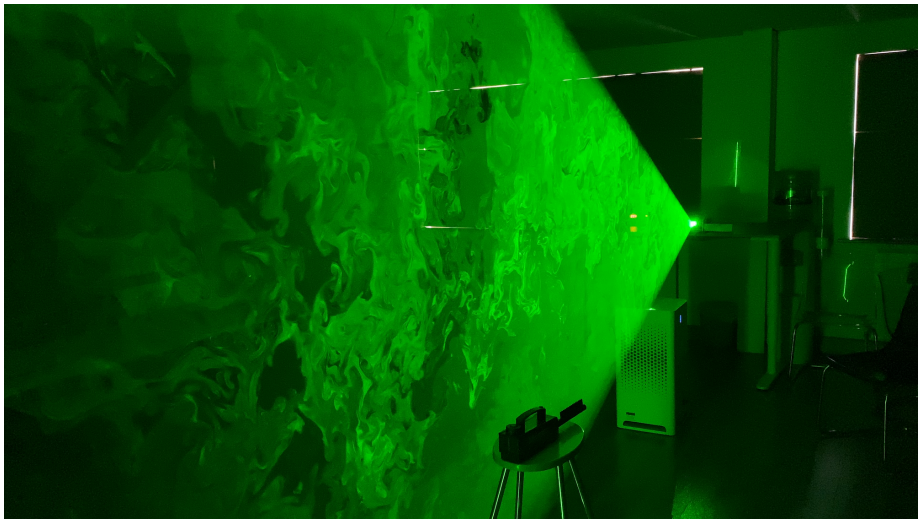

FIGURE 5. Photograph depicting the test setup used for measurements at the Camfil site. Note the laser expanded laser sheet in green, the aerosol generator in the foreground and the large amount of aerosol used to seed the flow. The City-M is observed below the laser source.

The second set of measurements was performed at the Mater hospital which considered the aerosol removal performance of the City-M in a smaller room. This involves recording the degree of light scattering from aerosol over several minutes compared to an untreated condition. The room used measured $4 \times 2.5 \times 2.26m$ and is representative of a typical hospital isolation room or a small office. A schematic of the configuration is shown in figure 6. The centre of the camera's field of view was positioned in the mid point of the room orthogonal to the laser sheet offset $1m$ resulting in a viewing diagonal of $0.5m$ with an 85 mm lens at $f/4$. Images (45 MP resolution) were automatically recorded at 10 second intervals over a 15 minute period. The resulting image data was averaged across the image frame and a time series produced. A particulate matter count was also recorded (Air image sensor) in unison to the image data. This sensor was placed on the table next to the City-H.

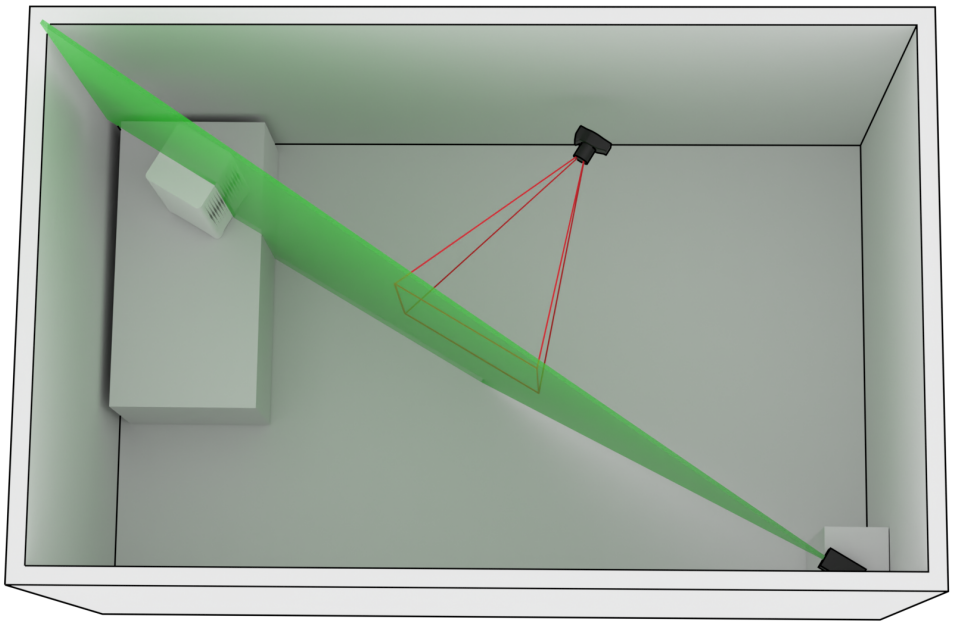

FIGURE 6. Schematic showing the optical arrangement for the aerosol tests in a $4 \times 2.5 \times 2.26m$ room. Note the position of the City-M at the top left, the laser source at the bottom right and the camera frustum shown in red.

3. Results and Discussion

3.1. **PIV Measurements of a single City-M.** A single unit City-M unit was tested in a large $(10 \times 10m)$ room. Placing the unit in the middle of the room eliminates any wall obstruction effects that may occur. The unit was placed on a desk that bounded the outflow jet on one side. All measurements were carried out at the maximum operational setting of the unit.

Initial measurements were performed at the inflow to the City-M unit to determine the flow velocity in close proximity to the unit.

The Aerogen nebuliser was positioned $1m$ away from the City-M at a height of $0.72m$ above the base of the unit. Aerosol consisting of $5\mu m$ saline solution was directed towards the unit. This will indicate the favoured flow direction and area over which air is received by the system. Figures 7 and 8 show two views of the same data. Figure 7 shows the velocity vectors (white) computed using ensemble averaged PIV (200 video frames) overlaid on a single representative video frame. It is more useful to plot this data in the form of a colour map as shown in figure 8 where the colour indicates the velocity magnitude of the flow interpolated between velocity vectors. The velocity magnitude data is mapped between 0 and $0.35m/s$ from blue to green to red. Shown also in this figure are streamlines which indicate the flow path and are tangent to the velocity vectors. From these figures is is clear that the flow velocity increases with proximity to the City-M, as expected due to the reduced pressure at the inlet. The region of highest velocity corresponds to the largest perforations in the front face of the unit. It is also notable that the flow is pulled downwards indicating that the unit is ingesting air from the greater surrounding volume above it rather than recirculating filtered exhaust flow immediately.

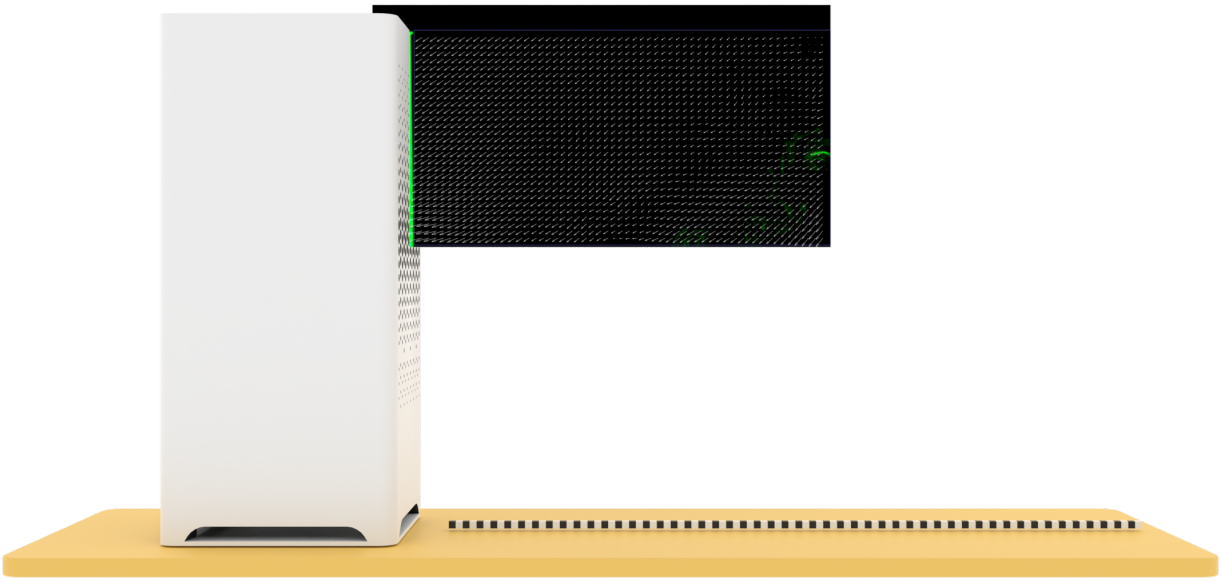

Figure 7. PIV measurement for the inflow to the City-M with an aerosol generator placed 1m to the right. Shown is the velocity field overlaid on a single video frame. Note also the 1m scale bar.

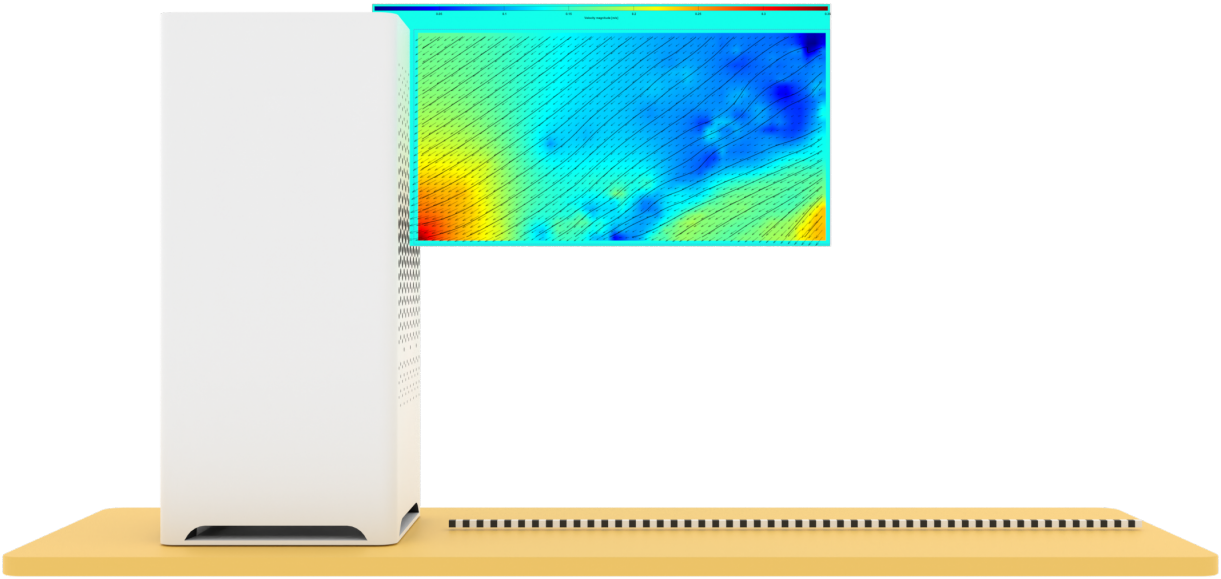

FIGURE 8. The data shown in figure 7 but coloured with the *jet* colour map over a velocity magnitude range form 0 to 0.35 m/s.

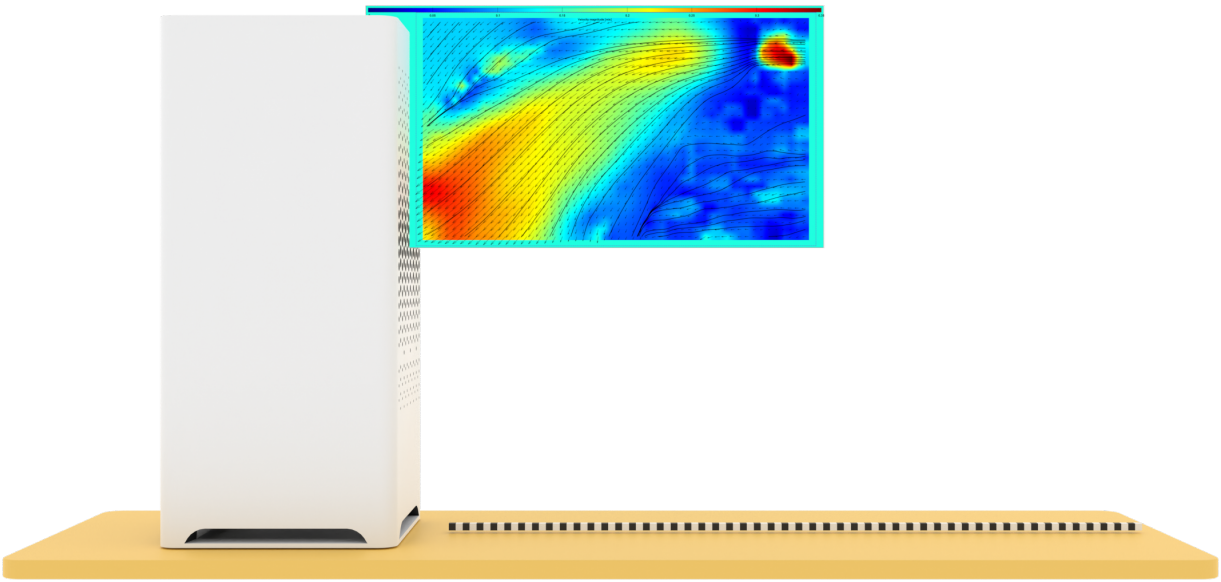

FIGURE 9. Inlet flow entrainment for $5\mu m$ aerosol generated $0.5m$ from the City-M inlet. The colour mapping is the same as in figure 8.

This test was then repeated with the horizontal distance to the nebuliser reduced to $0.5m$ as shown in figure 9. Similar results were obtained (note the 'hotspot' due to the aerosol flow exiting the nebuliser) which showed the same downwards accelerating flow towards the largest front face perforations. It is clear form these tests that the inflow of the City-M is capable of entraining the stream of aerosol flow effectively up to $1m$ away. This offers validity to the idea of supplementary personalised air purification [15] for scenarios such as dentistry where proximity is unavoidable [16]. However, for scenarios involving larger spaces and greater occupancy, like classrooms [17], understanding the wider effect is required.

The outflow jet was characterised next. Due to the positioning of the fan (figure 1) and the smaller area relative to the large inflow region the velocity here is expected to be larger. Here the camera's frame rate at 8K resolution was not sufficient to capture coherent particle motion for the fast moving air close to the City-M outlet however this was measured at approximately $0.5m/s$ using a handheld anemometer. The aforementioned smoke wand was placed in proximity to the outflow and a rake attachment used to generate a wide stream of tracer particles. The smoke is observed to travel along the tabletop surface in a turbulent manner as shown in figure 10. Streamlines are also shown in figure 10 as the particles can be tracked once the flow has sufficiently slowed as it loses kinetic energy to turbulence generation and viscosity. At a distance of $1.1m$ from the City-M, the streamlines are observed to lift up and form a vortex The velocity of the jet below the vortex is measured at $0.15m/s$. This behaviour is typical of jet flows as the high-speed flow is sheared against the surrounding mostly stagnant flow resulting in lateral spreading of the jet with vortex shedding along its periphery. In the absence of the table surface one would expect a vortex pair (corresponding to the laser sheet slicing through a vortex ring). No aerosol was observed at the City-M inflow during these tests as the aerosol was not left to circulate for a longer period of time.

Considering the observed inflow and outflow characteristics it is apparent that there is no immediate cross talk between the filtered and unfiltered air. The inflow stream is pulled downwards from above the unit while the outflow is expelled at a higher velocity.

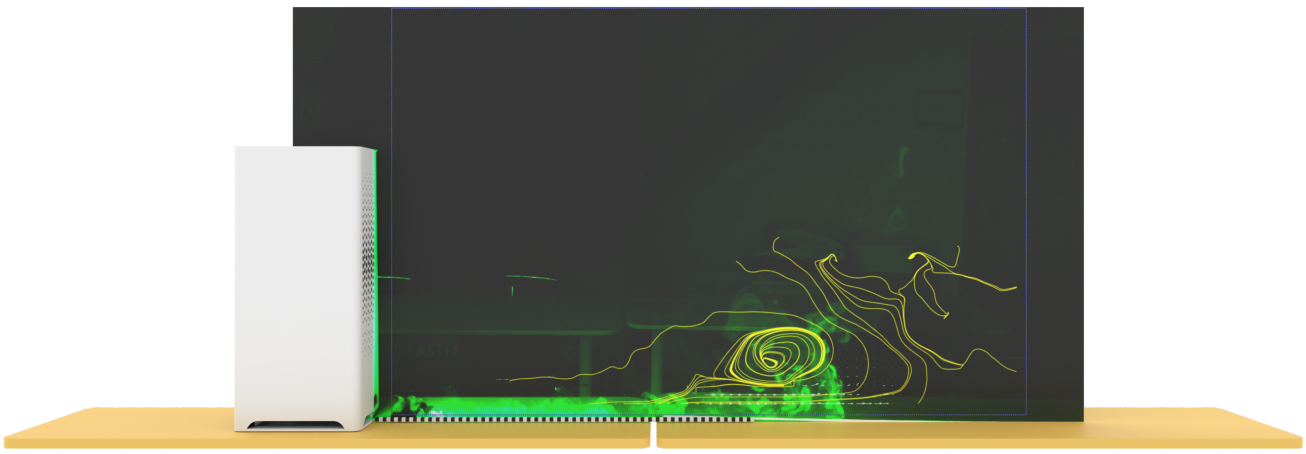

FIGURE 10. Exhaust jet flow exhibiting vortex shedding at $1.1m$ from the City-M

It is clear, however, that the City-M sets up contraflow streams of air. One would therefore expect a recirculating region of flow to occur due to incompressibility and mass conservation as the filtered clean air moving outwards and the unfiltered air bring pulled inwards act as a source and a sink. To test this the smoke wand's rake was placed $2m$ downstream of the exit jet and the aerosol left to disperse for some time. Shown in figure 11 is an image from the video sequence with the PIV colour map and streamlines overlaid. The position of the smoke wand at the extreme lower right of the image is visible. The colour map values are the same as in figure 8 corresponding to a range of $0 - 0.35m/s$. The streamlines clearly indicate a large recirculation region that spans $2m$ with the flow accelerating as it approaches the inflow to the City-M as per figures 8 and 9

It is notable that the configuration of the City-M results in the unfiltered air returning to the unit by travelling up and over any seated individuals sitting within its area of effect. This indicates the importance of understanding deployment location when considering the effect of such systems on room-scale flow dynamics.

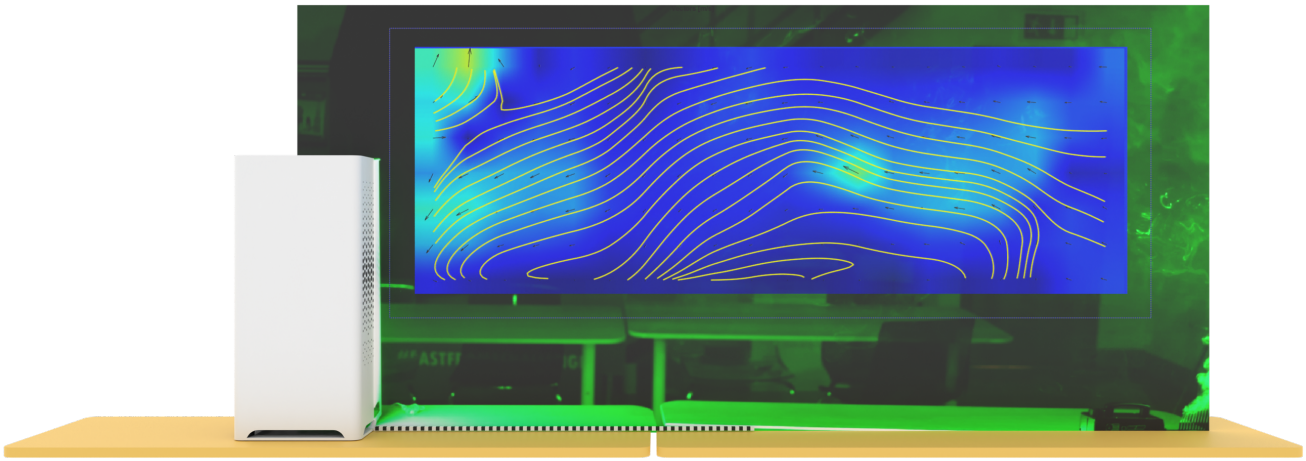

FIGURE 11. Large scale recirculation regions spanning $2m$ outwards from the City-M.

Tests were also performed with a pair of City-M units placed at various separation distances. These proved difficult to extract PIV data from due to limited testing time, further measurements may be required. Nevertheless one example was successfully processed as shown in figure 12 which depicts two City-M units placed $1.5m$ apart. The flow map in figure 12 shows a strong vortex in front of the leftmost unit. In this recording the flow has a bias to the left side and the test was not repeated with the smoke wand repositioned due to difficulty adequately illuminating the space close to the right unit. It is reasonable to infer that a similar contra-rotating vortex is present on the right side; further testing will verify this. In this scenario the outflow jets from each unit collide at the midpoint and are direct upwards and outwards. This turns the flow and it is drawn back to the inflow by the low pressure.

Such a configuration is not particularly practical in most scenarios as the units are too close together to be comfortable for anyone occupying the space. Considering the extent of the single unit recirculation zone observed in figure 11 it appears that this contra-rotating behaviour may be

sustained for a radius up to a $2m$ around the unit providing high-quality filtration for an $4 \times 4m$ room if placed in the centre.

Assuming a mean velocity along a recirculating streamline in figure 11 is $0.05m/s$ and the recirculating flow path can be approximated as an ellipse with major and minor axes of $2m$ and $0.72m$ respectively, the flow path is $4.5m$ in length. Consequently it is possible for a single City-M to filter the air along this path every 90 seconds.

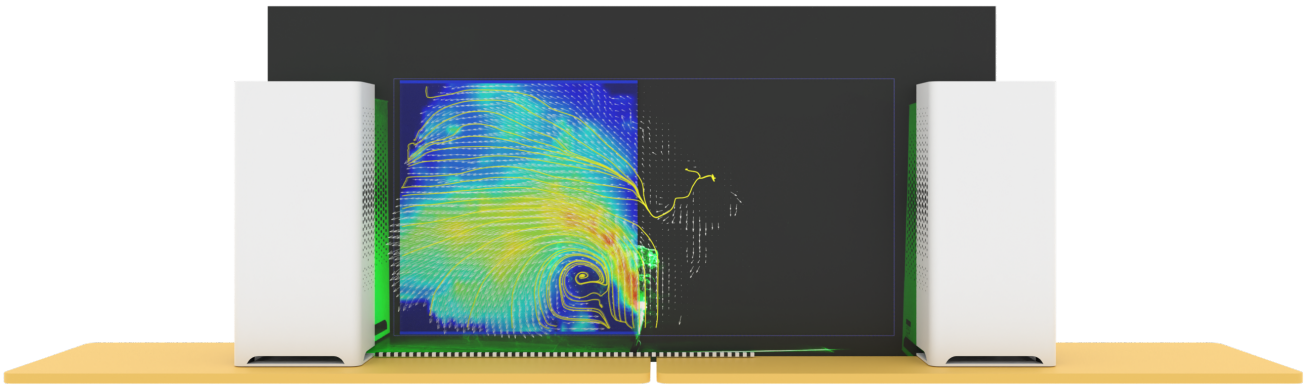

FIGURE 12. Recirculation zones between two City-M units placed $1.5m$ apart. Note that the smoke was entrained in the left recirculation zone for this test. The colour map is the same as in figure 8

3.2. **Aerosol reduction performance.** The second set of measurements concern the rate at which the City-M can reduce the aerosol content of the room air. This was measured in two ways, simultaneously. The first method used a Camfil Air Image Sensor which can quantify particulate matter PM1, PM2.5 and PM10 and log the data remotely. The second method employs Lorenz-Mie scattering of the laser light from the aerosol generated by the smoke wand to quantify the reduction in image intensity over time. The smoke wand was used to fill the test space (figure 6) for 30 seconds before each test. Note that this is a very large amount of aerosol and is not typical of an indoor environment where a continuous baseline of aerosol generation would be observed due to occupancy. As a result the amount of aerosol present will rapidly decay in all cases considered, however it is the relative decay rate that is of interest in the present study as it indicates the ability of the air purifier to remove particles from the environment. Coupled with the recirculation data above a greater understanding of the aerodynamic and filtration performance is possible.

Figures 13 and 14 show the particle counter data for two different scenarios. The first compares the untreated room (City-M powered off, black data series) to the treated state (City-M at maximum power setting, blue data series). The PM counts rapidly fall for the treated case with negligible particle count over a 160 second period. Compared to the untreated case, it takes > 400 seconds for a similar reduction.

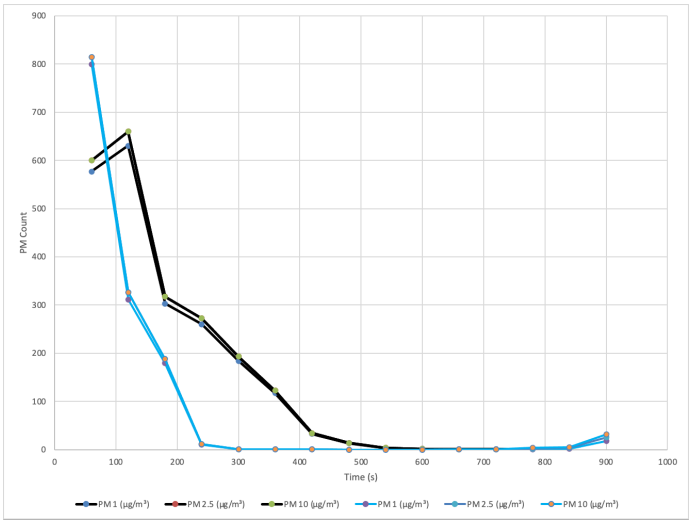

FIGURE 13. Particle count form the Camfil Air Image Sensor in the test space depicted in figure 6. Black data series indicate untreated aerosol and blue data series aerosol treated by the City-M at its maximum power setting.

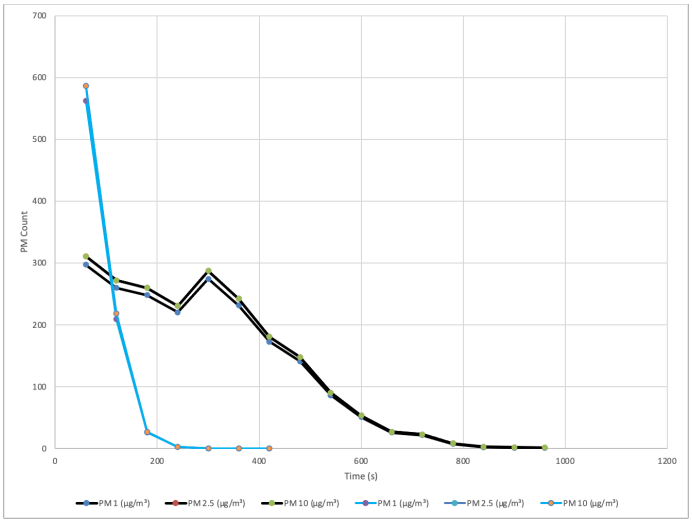

FIGURE 14. Particle count data as in figure 13 with additional buoyancy due to the placement of a heater in the centre of the test room.

In the second scenario, a small storage heater was placed into the room below the camera's field of view. The smoke generator was placed in the thermal plume of the heater giving the generated aerosol additional buoyancy. This increased the dissipation time for the untreated aerosol to 800 seconds while the treated aerosol was reduced to negligible levels in 200 seconds.

These observations are also observed in the laser scattering data, figure 15. Variation in the untreated (black) data show how effects such as buoyancy result in 600 – 800 second periods before the aerosol dissipates. For the treated cases where the City-M is operating at its maximum setting. the aerosol is cleared in 200 seconds consistently.

The particle counter data and the laser scattering data are well correlated showing that the point measurement from the former and the volume measurement of the latter. Based on these data and recirculation flow dynamics shown above, it is apparent that the City-M is an effective air purifier. Care must be taken when deploying such a device to precent cross contamination between individuals due to the recirculating air pattern. The vertical placement of the device is key to ensuring this.

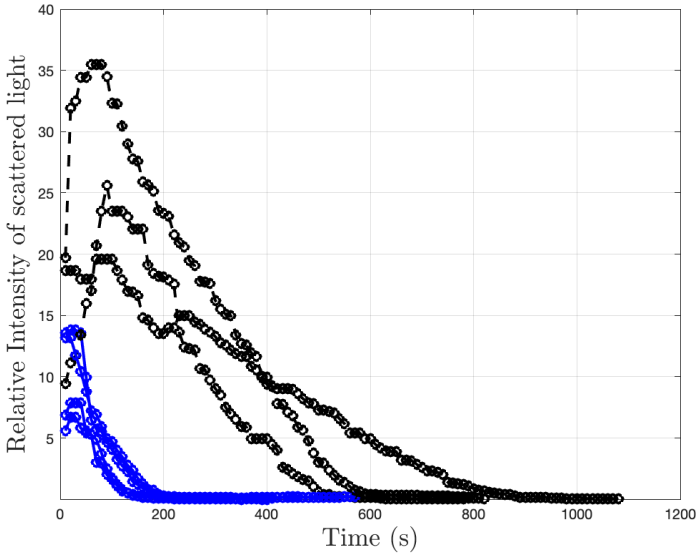

FIGURE 15. PM3

4. CONCLUSIONS

This study considered two sets of measurements. The first concerns the flow kinematics — how the flow moves to and from the device. The second set of measurements concerns the ability of the unit to rapidly reduce the amount of aerosol present.

The measurements establish that the outflow from the device is maintained separate from the inflow stream for at least $1m$ radially. A recirculation zone extending up to $2m$ is observed indicating that the device has a broad area of effect. Due to the outflow vents on all sides and the dynamics of low pressure inflows this is expected to provide robust air filtration in all directions. It is estimated that the flow circuit is completed in as little as 90 seconds. Since air is returned to the device up and over the outwards jet of filtered air (approximately $1m$ vertical spacing) care should be taken when during deployment as this may result in cross contamination via aerosol laden air. Placing pairs of City-M units opposite each other sets up a double-gyre flow pattern. This arrangement

may be useful for treating larger volumes. It also increases the upwards velocity of the air in the middle, however further testing of this arrangement is recommended.

The aerosol testing showed that the City-M offers robust and consistent filtration of large amounts of aerosol compared to no treatment. The City-M reduced particle sounds and observable laser scattering to negligible levels in less than 200 seconds. This represents a 3 to 4X improvement.

5. Acknowledgements

The author would like to thank Camfil for offering the use of their equipment and facilities for this testing and the Mater Misericordiae University Hospital for providing laboratory space. The author has not received any financial incentive for this work and Camfil has not influenced the findings herein.

References

[1] Renyi Zhang, Yixin Li, Annie L. Zhang, Yuan Wang, and Mario J. Molina. Identifying airborne transmission as the dominant route for the spread of covid-19. *Proceedings of the National Academy of Sciences*, 117(26):14857–14863, 2020.

[2] Trisha Greenhalgh, Jose L Jimenez, Kimberly A Prather, Zeynep Tufekci, David Fisman, and Robert Schooley. Ten scientific reasons in support of airborne transmission of sars-cov-2. *The lancet*, 397(10285):1603–1605, 2021.

[3] Chris Baraniuk. Covid-19: What do we know about airborne transmission of sars-cov-2? *BMJ*, 373, 2021.

[4] A C Fears, W B Klimstra, P Duprex, A Hartman, S C Weaver, K C Plante, D Mirchandani, J A Plante, P V Aguilar, D Fernández, A Nalca, A Totura, D Dyer, B Kearney, M Lackemeyer, J K Bohannon, R Johnson, R F Garry, D S Reed, and C J Roy. Comparative dynamic aerosol efficiencies of three emergent coronaviruses and the unusual persistence of sars-cov-2 in aerosol suspensions. *medRxiv : the preprint server for health sciences*, page 2020.04.13.20063784, 04 2020.

[5] Anand Srinivasan, Jayant Krishan, Sreekanth Bathula, and Yelia S. Mayya. Modeling the viral load dependence of residence times of virus-laden droplets from covid-19-infected subjects in indoor environments. *Indoor Air*, n/a(n/a), 2021.

[6] Amayu W Gena, Conrad Voelker, and Gary S Settles. Qualitative and quantitative schlieren optical measurement of the human thermal plume. *Indoor air*, 30(4):757–766, 2020.

[7] Lydia Bourouiba. Turbulent Gas Clouds and Respiratory Pathogen Emissions: Potential Implications for Reducing Transmission of COVID-19. *JAMA*, 323(18):1837–1838, 05 2020.

[8] Deepti Gurdasani, Nisreen A Alwan, Trisha Greenhalgh, Zoë Hyde, Luke Johnson, Martin McKee, Susan Michie, Kimberly A Prather, Sarah D Rasmussen, Stephen Reicher, et al. School reopening without robust covid-19 mitigation risks accelerating the pandemic. *The Lancet*, 397(10280):1177–1178, 2021.

[9] Rajesh K. Bhagat, M. S. Davies Wykes, Stuart B. Dalziel, and P. F. Linden. Effects of ventilation on the indoor spread of covid-19. *Journal of Fluid Mechanics*, 903:F1, 2020.

[10] Jianyun Lu, Jieni Gu, Kuibiao Li, Conghui Xu, Wenzhe Su, Zhisheng Lai, Deqian Zhou, Chao Yu, Bin Xu, and Zhicong Yang. Covid-19 outbreak associated with air conditioning in restaurant, guangzhou, china, 2020. *Emerging infectious diseases*, 26(7):1628–1631, 07 2020.

[11] A Melling. Tracer particles and seeding for particle image velocimetry. *Measurement science and technology*, 8(12):1406, 1997.

[12] Fulvio Scarano. Iterative image deformation methods in piv. *Measurement science and technology*, 13(1):R1, 2001.

[13] William Thielicke and Eize Stamhuis. Pivlab–towards user-friendly, affordable and accurate digital particle image velocimetry in matlab. *Journal of open research software*, 2(1), 2014.

[14] William Thielicke and René Sonntag. Particle image velocimetry for matlab: Accuracy and enhanced algorithms in pivlab. *Journal of Open Research Software*, 9(1), 2021.

[15] Bin Zhao, Yumeng Liu, and Chen Chen. Air purifiers: A supplementary measure to remove airborne sars-cov-2. *Building and environment*, 177:106918–106918, 06 2020.

[16] Bin Zhao, Na An, and Chen Chen. Using an air purifier as a supplementary protective measure in dental clinics during the coronavirus disease 2019 (covid-19) pandemic. *Infection Control and Hospital Epidemiology*, 42(4):493–493, 2021.

[17] Sebastian Burgmann and Uwe Janoske. Transmission and reduction of aerosols in classrooms using air purifier systems. *Physics of Fluids*, 33(3):033321, 2021.